



Cite this: DOI: 10.1039/d0mh00249f

Received 13th February 2020,  
Accepted 20th April 2020

DOI: 10.1039/d0mh00249f

rsc.li/materials-horizons

# Fluorescent chemo-sensors based on “dually smart” optical micro/nano-waveguides lithographically fabricated with AIE composite resins†

Meng-Dan Qian,<sup>a</sup> Yun-Lu Sun,<sup>\*b</sup> Zhi-Yong Hu,<sup>a</sup> Xiao-Feng Fang,<sup>c</sup> Jin-Long Zhu,<sup>d</sup> Xudong Fan,<sup>id</sup> Qing Liao,<sup>d</sup> Chang-Feng Wu<sup>id</sup>\*<sup>c</sup> and Hong-Bo Sun<sup>id</sup>\*<sup>e</sup>

Novel high-performance non-labeled fluoro-sensing micro/nano-optics require lithographically fabricable stimuli-fluorescence transductive materials well-tailored in molecular levels, towards superior processibility, stability, sensitivity, on-chip integration and portability, and real-time and *in situ* analysis. Here, aggregation-induced-emission fluorophores with oxetane groups (AIEoxes) and their covalently co-crosslinkable epoxy composites are customized for the fabrication of micro/nano-devices *via* single/multi-photon lithography. The oxetane modification increases the AIEoxe miscibility in the epoxy matrix (doping ratio up to 10 wt%), and consequently improves the as-formed devices' quality, stability, and fluorescence intensity and sensitivity. The multi-color-AIEoxe polymeric micro/nano-devices allow fluorescence-resonance-energy-transfer among AIEoxes, which enables sensitive and specifically spectral detection of VOCs. With the micro/nano-waveguide configuration, solvent-responsive AIE fluorescence and evanescent-field/refractive-index sensing enhance the AIE-fluorescent detection of trace organic solvents in aqueous solutions (detection limit, ~0.004% v/v, tetrahydrofuran/water) and their facile integration in functional micro/nano-systems like optofluidics.

## Introduction

Low molecular weight organics like volatile organic compounds (VOCs) are a common class of pollutants or impurities in air,

<sup>a</sup> State Key Laboratory of Integrated Optoelectronics, College of Electronic Science and Engineering, Jilin University, 2699 Qianjin Street, Changchun 130012, China

<sup>b</sup> Department of Biomedical Engineering, University of Michigan, Ann Arbor, MI 48109, USA. E-mail: yunlus@umich.edu

<sup>c</sup> Department of Biomedical Engineering, Southern University of Science and Technology, Shenzhen, Guangdong 510855, China. E-mail: wucf@sustech.edu.cn

<sup>d</sup> Beijing Key Laboratory for Optical Materials and Photonic Devices, Department of Chemistry, Capital Normal University, Beijing 100048, China

<sup>e</sup> State Key Laboratory of Precision Measurement Technology and Instruments, Department of Precision Instrument, Tsinghua University, Beijing 100084, China. E-mail: hbsun@tsinghua.edu.cn

† Electronic supplementary information (ESI) available. See DOI: 10.1039/d0mh00249f

### New concepts

The development of luminescent micro/nano-optics depends heavily on dye innovations with good luminescence properties. Different from traditional dyes that suffer from luminescence quenching at a high concentration, an aggregation-induced emission luminogen (AIEgen) is a novel material emitting strong luminescence in the solid state by restricting the intramolecular motions, making it a potential candidate in solid micro/nano-optics fabrication. Here, we propose a novel strategy to customize active micro/nano-optics using a “real” photoresist containing an SU-8 polymeric matrix and oxetane group decorated AIE molecules (AIEoxes) *via* single/two photon lithography. The covalent crosslinking property of AIEoxes together with SU-8 guarantees a high doping ratio (up to 10 wt%) as well as fabricable feasibility. By virtue of the fluorescence response of AIEgens to organic solvent stimuli, the constructed microstructures can be used as monochromic and multicolor ratiometric sensors to detect organic solvents. Furthermore, fabricated micro-waveguides show improved detection sensitivity due to the dual effects of the AIEgen fluorescence response effect and the evanescent refractive-index waveguide effect. This work not only offers new ideas for the material processing field but also provides promising opportunities for integrated optics for low-cost, real-time and *in situ* organic pollutant analysis.

water, or solvent products, bringing about increasing harm to the natural environment, human health, and quality control of chemical products.<sup>1</sup> Gas chromatography (GC), often coupled with mass spectrometry, is currently the most frequently used method of VOC analysis especially for in-lab operation and gas samples. Nevertheless, sensitive direct detection of VOCs and other organics in liquid hybrids (*i.e.*, aqueous or solvent solutions), particularly its facile, real-time, and *in situ* field implementation, is still challenging due to their molecular similarity, time/effort-consuming sample collection or processing before/during GC, and the large size of common GC systems.<sup>2–4</sup> Aiming to solve the above issues, strategies based on functional integrated optics promisingly provide novel opportunities for the trace-amount detection of these low molecular weight organics in air, water, or solvents.<sup>5,6</sup> “Smart” optical materials (*e.g.*, polymers, fluorescent dyes, *etc.*) responsive to VOCs enable passive and

active optics for sensitive VOC sensing or detection.<sup>7,8</sup> For instance, a refractive-index passive VOC optical sensor is constructed with a detection limit of  $\sim 10$  ppb *via* a 150  $\mu\text{m}$ -diameter optical fiber coated with a VOC-responsive polymer membrane, whereas it still demands improvement of its integration, stability, and especially response time.<sup>9</sup> Furthermore, efforts are still in high demand to implement on-chip integratable micro/nano-optic devices towards optofluidics facilely functionalized with superior signal read-out, sensitivity, recognizability, portability, and real-time and *in situ* capabilities of VOC detection and monitoring directly in liquid phases.

Current fluorescent VOC (or trace water in solvents) sensors are mainly based on aggregation caused quenching (ACQ) fluorophores (*e.g.*, Nile-red and carbon-dots) dispersed in VOC (or water) responsive matrices as responsive indicators.<sup>10,11</sup> The ACQ phenomenon obstructs the device fabrication with a high amount of doped fluorescent sensing components and therefore their detection signal intensity and sensitivity, as well as further realization of on-chip integratable VOC sensors (*i.e.*, VOC monitoring optofluidics).<sup>12</sup> Different from ACQ, aggregation induced emission (AIE) is associated with restriction of intramolecular motions (RIM) of specific fluorophores, leading to much stronger fluorescence through molecular-environment restriction (*e.g.*, aggregation, solidification, or matrixing in solid composites), and has been developed to be a novel and improving option for on-chip device construction.<sup>13,14</sup> More importantly, the special working mechanism of AIEgens facilitates their more sensitive responses towards stimuli-fluorescence transducers.<sup>15</sup> Prof. Tang's and Prof. Jiang's groups successfully proved that AIE-based fluorescent VOC sensing shows novel potential of improving active optical detection of VOCs, even though mostly only dispersions,<sup>16</sup> films,<sup>17</sup> or micro-pattern arrays are applied.<sup>18</sup> Particularly, recognizable detection, as important as sensitivity, is exhibited by principle component analysis (PCA) of monochromatic AIE materials' responses to VOC vapors in the latest work of Prof. Jiang's group,<sup>19</sup> while fluorescence-resonance-energy-transfer (FRET) may be also applicable towards specifically recognizable fluoro-chromatic spectral detection but with better self-calibration and easier read-out.<sup>20,21</sup>

Herein, we propose a novel strategy to build active integratable optics (*i.e.*, micro/nano-waveguides) using specifically tailored AIE epoxy composite resins as building blocks, and organically combine the special stimulus-fluorescence transduction of AIE molecules, FRET-aided fluoro-chromatic effect, and evanescent/refractive-index waveguide effect to improve the recognizability and detection of VOCs directly in aqueous hybrids. Three element-color (*i.e.*, red, green and blue) AIE fluorophores are purposely modified with oxetane groups to improve the miscibility and doping ratio (up to 10 wt%) in epoxy resins. Covalently co-crosslinkable AIEoxes/epoxy composite resins are single/two-photon lithographically fabricated into active polymeric micro/nano-patterns and optical micro/nano-waveguides with high morphology/device quality and in-solvent stability in both structure and fluorescence for liquid-phase operation.<sup>22</sup> Good applicability to photo-lithography, the most widely used micro/nano-fabrication method, contributes to their facile integratable

construction in micro/nano-systems like optofluidics.<sup>23</sup> In particular, two-photon lithography (*i.e.*, femtosecond laser direct writing (FsLDW)) significantly facilitates the free-design and on-demand fabrication of active sub-micro/micro-waveguides,<sup>24,25</sup> which are expected to show a quick response and high sensitivity towards VOCs because of the high volume-surface ratio, polymer swelling and AIE "de-fixing".<sup>19,26,27</sup> FRET among multiple AIEoxe components inside polymeric micro/nano-patterns enables their spectral detection of VOCs (*e.g.*, acetone, tetrahydrofuran, ethanol and dimethyl-formamide here) and improved sensitivity, accuracy and precision compared to monochromatic sensing. Furthermore, polymeric swelling, solvent-responsive AIE fluorescence, and evanescent-field/refractive-index sensing *via* optical micro/nano-waveguiding enhance each other, as a "dually smart" strategy with easy read-out and integration, to detect trace-amount VOCs directly in liquid phases (*i.e.*, a detection limit of  $\sim 0.004\%$  v/v (tetrahydrofuran (THF)/water) as a demonstration here).

## Results and discussion

Three types of AIEoxes emitting blue, green or red fluorescence (bAIEoxe, gAIEoxe, and rAIEoxe) are designed and synthesized here with the method reported in our previous work.<sup>28</sup> As illustrated in Fig. 1a, the AIEoxe molecules are constructed based on tetraphenylethylene (TPE) and its derivatives. By rationally controlling

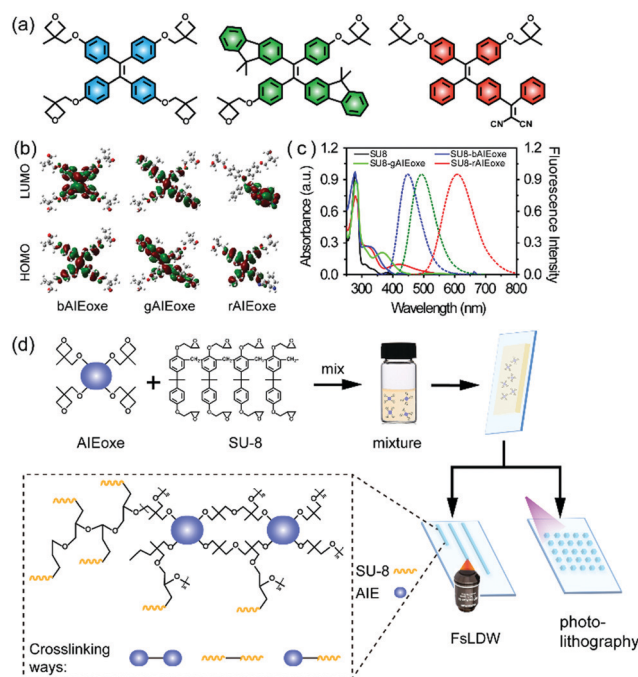


**Fig. 1** Schematic of the designed AIEoxe structures and the fabrication process using single/two-photon lithography. (a) Chemical structures of the three AIEoxes. (b) Computed frontier molecular orbitals of the AIEoxe molecules. (c) UV-vis absorption spectra and fluorescence spectra of SU-8/AIEoxe composite films. (d) Schematic illustration of the preparation and fabrication of AIEoxe incorporated micro/nano structures by means of FsLDW induced two photon polymerization and UV photolithography; the polymerization mechanism among AIEoxe molecules and the SU-8 resin in the fabrication process (dashed box).

the conjugation length and intra-molecular energy transfer process, AIEoxe molecules emit from blue to red. The introduced fluorene and cyano groups in gAIEoxe and rAIEoxe lead to the decrease of the energy gap ( $E_{\text{gap}}$ ) and further the red shift of the absorbance and emission spectra (Fig. S1, ESI<sup>†</sup>). The computed electronic cloud distribution demonstrates that the electrons of AIEoxes mainly delocalize over the aromatic TPE frameworks without interactions with oxetane groups, indicating that the modified oxetane groups have little influence on the photophysical properties (Fig. 1b).

We apply SU-8, a frequently used commercial photoresist for a demo, as the polymer matrix because of its excellent chemical stability and fabricable properties.<sup>29</sup> A pure SU-8 film shows almost no photo-luminescence emission. AIEoxe molecules are doped in the SU-8 matrix as efficient luminescent materials. The absorption and photo-luminescence spectra of SU-8/AIEoxe composite films and the AIEoxe solution are similar (Fig. 1c and Fig. S2, ESI<sup>†</sup>), indicating that the SU-8 matrixing causes no obvious change in the photophysical properties of AIEoxe molecules. The preparation of the AIEoxe-doped SU-8 composite resin and its device-fabrication process through single/two-photon lithography are illustrated in Fig. 1d. The SU8/AIEoxe composite resin is spin-cast into homogeneous and uniform thin films, which can be further fabricated into various photoluminescent micro/nano-structures by UV photo-lithography or two-photon-polymerization FsLDW. Thanks to the AIE features, the luminescence intensity of AIEgens become stronger in the as-prepared solid SU-8 film with a doping ratio up to 10 wt% (Fig. 2a and Fig. S3, ESI<sup>†</sup>). The fluorescence quantum yield of the AIEoxes in solid films is measured to be  $\sim 68.8\%$ ,  $\sim 57.7\%$  and  $\sim 33.8\%$ , respectively (Fig. S4, ESI<sup>†</sup>). By contrast, conventional dyes, for instance rhodamine B (RhB), experience an obvious ACQ effect with the highest doping ratio of  $\sim 1$  wt% in the SU-8 matrix (Fig. 2b and c). The distorted structures of the AIEoxes hamper the strong intermolecular interactions induced by  $\pi$ - $\pi$  stacking, contributing to the high photo-luminescence efficiency at high doping concentrations. Besides, there is no energy transfer process observed between the AIEoxes and epoxy SU-8 matrix since the lifetimes of the AIEoxes in SU-8 show no obvious change in comparison to the pure AIE solids (Fig. S5, ESI<sup>†</sup>).

Tolerance to solvents, heat, and light exposure is essential for the high-quality photo-lithographic fabrication and practical operation of as-made materials and devices. Rather than simply blending, the matrix (*i.e.*, SU-8) and functional components (*i.e.*, AIEoxes) in the composites here can covalently crosslink into solvent-tolerant micro/nano-devices. The AIEoxes are purposely modified with oxetane groups, making their SU-8 composites “real” photoresists with covalent co-crosslinking capability. Thus, the AIEoxe molecules are more stably loaded in the fabricated structures than unadorned ones, which is important for their compatibility with photolithography using solvents and developers, as well as VOC sensing directly in liquid phases. Handwritten patterns made with SU-8/AIEoxe and SU-8/undecorated-dye (*i.e.*, bAIE, RhB, and fluorescein) inks are used for the comparative investigation of in-solvent stability (Fig. 2d and Fig. S6, ESI<sup>†</sup>). The morphology and fluorescence brightness of the cured patterns (250 W mercury lamp for 5 s) are studied during long-time

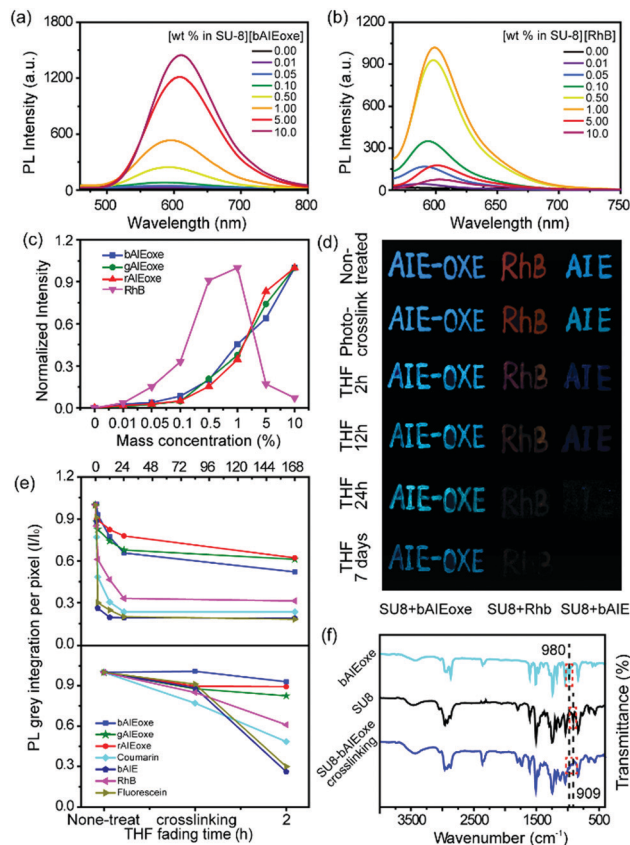


Fig. 2 The typical AIE traits of the three AIEoxes in composite SU-8 films and the covalent crosslinking phenomenon. (a and b) Fluorescence spectra of bAIEoxe and RhB in the SU-8 matrix with various doping concentrations. (c) The plot of normalized fluorescence intensity against different doping concentrations of AIEoxes and RhB. (d) Chemical stability of the crosslinked handwritten patterns containing bAIEoxe, RhB and bAIE molecules against THF treatment. (e) Normalized grey-level values of the fluorescent handwritten patterns against different THF treatment time. The upper graph describes the fluorescence intensity change for a week, and the lower one is the detailed curve of the first two hours. (f) FTIR spectra of bAIEoxe molecules and SU-8 before and after crosslinking.

immersion in THF, a solvent that dissolves well uncrosslinked SU-8 prepolymers and these dye molecules. As shown in Fig. 2d and Fig. S6 (ESI<sup>†</sup>), a large part of the undecorated dyes physically blended in the patterns are quickly dissolved into THF from the SU-8 matrix in the first 2 h. The polymer patterns' fluorescence sharply fades down to only  $\sim 30\%$  of the initial intensity after 2 h THF immersion, and finally becomes dim and even invisible after 24 h (grey-level integrated intensity in Fig. 2e). In contrast, after a quick but slight washing away of some uncrosslinked AIEoxes, the patterns crosslinked with AIEoxes show superior resistance to THF. Their fluorescence brightness stays stably at  $\sim 60\%$  of the original value after THF immersion for 7 days or even longer. The photo-crosslinking of AIEoxes with SU-8 is further verified by Fourier-transform infrared (FTIR) spectroscopy. The characteristic peaks of oxetane groups in the AIEoxes ( $980\text{ cm}^{-1}$ ) and epoxy groups ( $908\text{ cm}^{-1}$ ) in SU-8 disappear after UV irradiation, accompanied by the broadening of the band of the acyclic ether linkage at  $1010\text{--}1130\text{ cm}^{-1}$  (Fig. 2f).<sup>30,31</sup> The photo-crosslinking feature of the

AIEoxes with the SU-8 resist significantly improves the fabricated patterns and active devices' in-solvent stability.

Apart from the chemical stability, the photo-stability of responsive dyes is another crucial parameter in the sensing process. As an excessive test, the photo-stability of the composite film is subsequently measured under continuous exposure to a 150 W Xe-lamp for about 1 h. As shown in Fig. 3a and b, rAIEoxe in SU-8 exhibits the best photo-stability, maintaining about 93% of its initial fluorescence intensity after 1 h continuous irradiation. bAIEoxe and gAIEoxe in SU-8 are not as stable as rAIEoxe, and only achieve 40% and 48% of the initial state, respectively. In addition, it is worth noting that AIEoxe molecules in their bare films generally suffer more serious photo-bleaching than that in the SU-8 matrix with the prolongation of the exposure time (Fig. S7, ESI<sup>†</sup>). The improved photo-stability of SU-8/AIEoxe can be attributed to the good encapsulation of the SU-8 matrix, which effectively impairs the photo-destruction process during

illumination.<sup>32</sup> In fact, the AIEoxes show excellent photo-stability that is comparable to and even slightly better than some commercial dyes such as RhB and coumarin, benefiting their functioning in as-fabricated optically active micro/nano-devices. Besides, the heat endurance of the composite resin film is also studied to eliminate probable negative influences caused by the heat effect during the fabrication process. The sample is subjected to 15 thermal cycles by being alternately heated to 90 °C and cooled to 30 °C. The maximal cycling temperature is 90 °C since epoxy resins are usually heated to this temperature for pre-/post-baking during the photo-lithography. The fluorescence intensity of the AIEoxe becomes weak as the sample is gradually heated to 90 °C (Fig. S8, ESI<sup>†</sup>) because of the increasing nonradiative transition process caused by thermally activated molecular motions,<sup>33</sup> whereas it recovers to the original fluorescence intensity when the sample is cooled to room temperature (Fig. 3c). The fluorescence reversibility of SU-8/AIEoxe towards thermal stimuli also makes it a promising candidate for fluorescence based thermal sensors.<sup>34</sup>

The single/two-photon lithographical micro/nano-fabrication of these SU-8/AIEoxe resins with 10 wt% AIEoxe doping fraction is well implemented. As a demonstration, we employ single-photon lithography to customize large-area 2D polygonal arrays (Fig. 3d and Fig. S12, ESI<sup>†</sup>). For the FsLDW process, a series of processing parameters (laser power, scanning step and scanning rate) are optimized (Fig. S9–S11, ESI<sup>†</sup>) to ensure the good surface smoothness and as-designed 3D free-form construction of micro-structures. Various complicated 2D micro-patterns such as the badge and name of Jilin University (Fig. 3f), as well as delicate 3D micro-crabs, are well fabricated with high spatial resolution (Fig. 3e). All the micro-structures have the expected morphology as designed, and emit uniformly bright fluorescence under UV excitation. The oxetane modification of AIE molecules decreases the negative impact of the high doping ratio on the morphology of the fabricated structures.

The network inside polymer micro/nano-structures is covalently inserted with AIEoxes, so that its swelling or shrinking tunes the intermolecular rotations of AIEgens and their fluorescence emission.<sup>19,26,27</sup> It is noted that the bulk film can be readily quenched under the stimulus of saturated THF vapor (Fig. S13, ESI<sup>†</sup>), proving the sensitive response of the SU-8/AIEoxe composites towards VOCs. Micro-cube ( $20 \times 20 \mu\text{m}^2$ ) arrays containing monochromatic AIEoxe and multi-AIEoxes are then fabricated respectively for VOC sensing in the liquid phase. Considering that the operating time during the sensing assay is short ( $< 4$  s per spectrum test and  $< 1$  min per device in total) with low exposure and negligible photobleaching, the fluorescence quenching of microdevices can be roughly attributed to the organic solvents (Fig. S14, ESI<sup>†</sup>). Fig. S15–S17 (ESI<sup>†</sup>) show the changes in the fluorescence spectra of three monochromatic SU-8/AIEoxe micro-structures in response to various VOCs (*i.e.*, acetone, EtOH, THF and DMF). Generally, the  $I_0/I$  value increases linearly with the amount of VOCs at low concentration (Fig. 4b), following the Stern–Volmer relation. The fluorescence tends to be stable after  $\sim 2\%$  v/v despite the continuous addition of VOCs (Fig. 4a and Fig. S18, ESI<sup>†</sup>). The fluorescence quenching degree is related to the

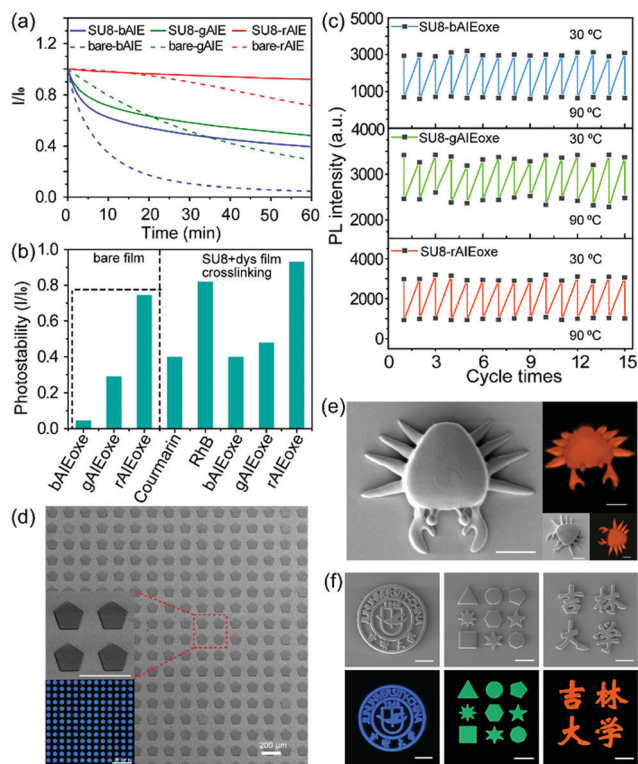


**Fig. 3** Characterization of the photophysical stability of the AIEoxes in the polymeric matrix. (a) Photostability comparison between SU-8/AIEoxe composite films and bare AIEoxe films. The samples were spin-coated on glass and were irradiated under continuous illumination with a 150 W Xe-lamp for 1 h. (b) The remaining fluorescence intensity of the luminous dyes after 1 h irradiation in comparison with their initial intensity. (c) The thermal stability of the three AIEoxes in the SU-8 matrix by alternately recording the fluorescence intensity at 30 °C and 90 °C for 15 cycles. (d) Large-area 2D micro-structure arrays generated by UV photolithography. The insets are the fluorescence image and enlarged view of local microstructures. The scale bar is 200  $\mu\text{m}$ . (e) SEM and fluorescence images of 3D micro-crabs created by femtosecond laser induced photopolymerization. The insets are the same micro-crabs with various view angles. The scale bar is 10  $\mu\text{m}$ . (f) SEM and fluorescence images of various micro-patterned examples *via* the FsLDW method. The scale bar is 20  $\mu\text{m}$ .

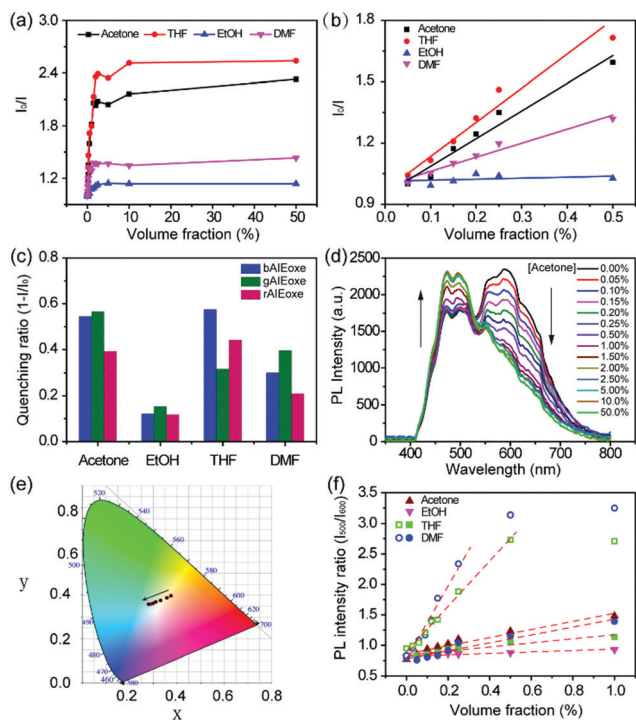


**Fig. 4** The fluorescence response of the fabricated micro-patterns to VOC solvent stimuli. (a) Relative fluorescence intensity change ( $I_0/I$ ) of micro-cubes containing bAIEOxe after treatment with aqueous solutions containing different organic solvents ranging from 0% to 50% v/v. (b) The detailed plot of (a) with the VOC amount under 0.5% v/v. (c) The final quenching ratio ( $1 - I/I_0$ ) of the monochromatic AIEOxe microstructures after treatment with 50% v/v VOC aqueous solutions. (d) Fluorescent emission spectra of the fabricated three-AIEOxe mixed micro-cubes under treatment with various amounts of acetone in water. (e) Chromaticity coordinate diagram with respect to the emission color corresponding to the fluorescence spectra in (c). (f) Plot of the intensity ratio of two typical emission peaks ( $I_{500}/I_{600}$ ) versus VOC content in water. The solid scatter-plots represent the spectral behavior of 20  $\mu\text{m}$  microstructures while the hollow ones are the spectral changes of the microwire with a smaller size (1  $\mu\text{m}$ ) in response to VOCs.

solvent polarity induced polymeric swelling.<sup>27,35</sup> In comparison to the poorest SU-8 polymeric swelling capacity of EtOH, the other three solvents (*i.e.*, acetone, DMF, and THF) have a polarity closer to the polymer matrix, and penetrate into and swell the SU-8/AIEOxe network much more effectively to specifically activate the intramolecular motions of AIEOxe molecules and consequently diminish their fluorescence emission (Fig. 4c).

The absolute-intensity fluorescent VOC sensing *via* monochromatic microstructures is susceptible to external factors caused by instruments and testing processes. Thus, “multi-component” FRET SU-8/AIEOxe micro-structures containing three AIEOxe molecules are constructed for ratiometric luminescent VOC sensing, which is thought to be more reliable and accurate since FRET fluorescence spectra, as the sensing signal, include two or three main peaks to enable self-referencing and self-calibration to reduce system errors or fluctuations. The “mixed” microstructures (bAIEOxe : gAIEOxe : rAIEOxe = 1 : 1 : 1; original CIE coordinates: (0.37, 0.39)) emit a bright salmon colour under UV light. As shown in Fig. 4d, three typical emission peaks from bAIEOxe, gAIEOxe and

rAIEOxe can be simultaneously observed at 475 nm, 500 nm and 600 nm, respectively, in the fluorescence spectrum. Theoretically, an efficient FRET process is permitted from b/gAIEOxe to rAIEOxe because the emissions of b/gAIEOxe overlap well with the absorbance spectrum of rAIEOxe and they are extremely close to each other (Fig. S19, ESI<sup>†</sup>).<sup>36</sup> When treated with VOC molecules in the liquid phase, the red emission at 600 nm fades, accompanied by the gradual increase of the blue (475 nm) and green (500 nm) emissions (Fig. 4e and Fig. S20, ESI<sup>†</sup>). These special spectral variations typically indicate the existence of resonance energy transfer. The presence of VOCs (*i.e.*, acetone as a demonstration in Fig. 4) induces the visible fluorescence color change of the micro-structure from the original salmon to cyan (CIE coordinates: (0.25, 0.35)), which enables the visual detection of VOCs (Fig. 4e).<sup>37</sup> The intensity ratio of the green (500 nm) and red (600 nm) emission ( $I_{500}/I_{600}$ ) vs. the acetone content within 1% v/v is depicted in Fig. 4f. Generally, the ratio of  $I_{500}/I_{600}$  increase linearly as the VOC content rises up to 1% in water. The limits of detection (LOD) of monochrome and multicolor micro-patterns are calculated and listed in Table S1 (ESI<sup>†</sup>). According to the data, the LOD of the multi-color structures is generally lower than the monochromatic ones since the FRET process is highly sensitive to the luminescence of the fluorophores involved and their enlarged distances associated with polymeric swelling. The fluorescence color change is visually recognizable and of help for convenient on-site VOC detection. In fact, the VOC induced polymeric swelling effect is the main reason for the fluorescence spectra variations for both the monochromatic and fluoro-chromatic microstructures. The only difference is that the monochromatic microstructures show only fluorescence quenching under VOCs, whereas the multi-color fluoro-chromatic system not only experiences fluorescence quenching but also has an energy transfer process which leads to variations of two emission peaks. Particularly, reducing the micro-devices’ sizes improves their sensitivity to VOCs because of the larger surface-to-volume ratio. Furthermore, the sensitivity of the microstructures increases 2–3 fold as their sizes decrease from 20  $\mu\text{m}$  to 1  $\mu\text{m}$  (Fig. 4f and Fig. S21, ESI<sup>†</sup>), or even higher if using FSLDW-fabricated nano-devices.<sup>38</sup> As a demo here, the VOC LOD of 1  $\mu\text{m}$  microwires is significantly enhanced to  $\sim 0.007\%$  v/v with this “multi-component” FRET method (Table S1, ESI<sup>†</sup>).

The high-quality lithography with these functional SU8/AIEOxe resins has practical potential to further build superior active micro/nano-optics (*e.g.*, waveguides) for optimized integration capability and sensing performance enhancement.<sup>39,40</sup> On low-refractive substrates (fused quartz sheets) we apply FSLDW for low-cost and facile on-chip fabrication of various AIEOxe-containing SU-8 micro/nano-wires with a smallest linewidth of  $\sim 100$  nm if needed.<sup>38</sup> In Fig. 5a and Fig. S22 (ESI<sup>†</sup>), the as-fabricated microwires show the configurations as designed with a  $\sim 2$   $\mu\text{m}$  linewidth and  $\sim 0.9$   $\mu\text{m}$  height in the comprehensive consideration of both waveguiding/sensing performances and test operability under an optical microscope. The surface quality of the devices is good enough for optical application ( $R_a$ ,  $\sim 4.4$  nm) along with the uniform AIEOxe distribution and fluorescence intensity. The microwires exhibit excellent optical waveguiding performance,

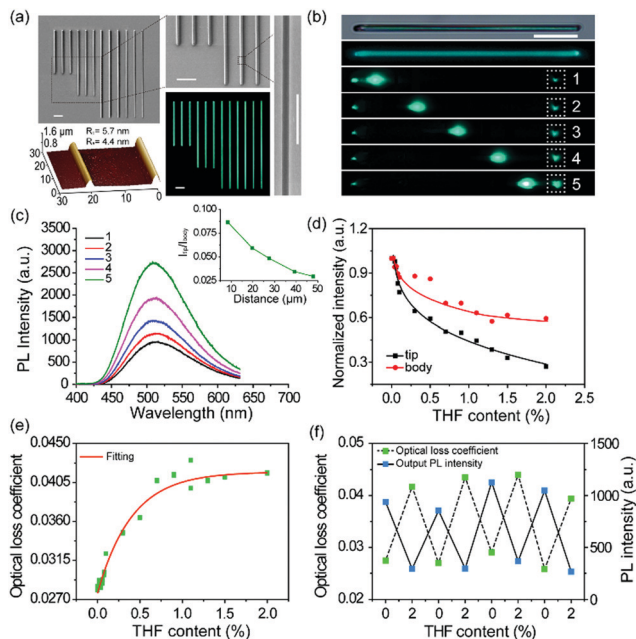


**Fig. 5** Fabrication and performance characterization of waveguides in aqueous VOC sensing. (a) The morphology of microwires characterized by SEM, AFM and fluorescence microscopy. The scale bar is 10  $\mu\text{m}$ . (b) Bright-field and fluorescence micrograph images of a gAIEoxe doped microwire by exciting different positions with a laser beam (400 nm). The scale bar is 10  $\mu\text{m}$ . (c) Spatially resolved PL spectra recorded from the right tip of the microwire with different propagation distances between the excitation spot and right tip of the microwire shown in (b). The inset is the relation of  $I_{\text{tip}}/I_{\text{body}}$  against the propagation distance. (d) Normalized fluorescence intensity change of the microwire (exciting spot and tip) after exposure to aqueous solutions with increasing THF content. (e) The optical loss coefficient change of the microwire in aqueous solutions containing various amounts of THF. (f) Reversible measurement of the micro-wire's fluorescence intensity at the output tip and optical loss coefficient when exposed to THF aqueous solution (2%) and heat treatment at 90  $^{\circ}\text{C}$  for 15 min (0%).

which is investigated by spatially resolved photoluminescence (PL) spectra. Fig. 5b and c show the fluorescence microscopic images of an exciting laser spot focused at different positions along the wire, and the corresponding spatially resolved PL spectra obtained from the right end labeled with 1, 2, 3, 4, and 5, respectively. The optical loss coefficient of the SU-8/bAIEoxe, SU-8/gAIEoxe and SU-8/rAIEoxe waveguides is calculated to be 0.0309  $\text{dB } \mu\text{m}^{-1}$ , 0.0274  $\text{dB } \mu\text{m}^{-1}$  and 0.0412  $\text{dB } \mu\text{m}^{-1}$ , respectively (Fig. S23–S25, ESI $^{\dagger}$ ), which are even lower than the optical loss of some reported organic crystalline micro-rods and organic/inorganic waveguides.<sup>41</sup> The FsLDW-guaranteed device quality and small self-absorption of AIEoxes contribute to the excellent waveguiding property of these microwires.

The waveguiding of AIEgen fluorescence in the active microwires enables amplified fluorescence quenching to improve the sensitivity *via* the polymeric micro-wires' VOC-induced swelling, evanescent field of propagated light and high surface-to-volume ratio.<sup>42,43</sup> Here, we use the SU-8/gAIEoxe microwires to detect a trace amount of THF in liquid hybrids. As shown in Fig. 5d and Fig. S26 (ESI $^{\dagger}$ ), the fluorescence intensity of the microwires at

the exciting point (position 1 in Fig. 5b) decreases by 50% as the content of THF increases to 2% v/v in its aqueous solution. Meanwhile, the corresponding output signal at the right tip of the microwire suffers more severe quenching, finally remaining at only 25% of its initial PL intensity, with an amplified fluorescence quenching response and improved sensitivity to THF. The different fluorescence quenching degree between the microwire body and output tip is attributed to the optical loss variation during the addition of THF (Fig. 5e). The optical loss coefficient of the microwire increases from 0.0274  $\text{dB } \mu\text{m}^{-1}$  to 0.0417  $\text{dB } \mu\text{m}^{-1}$  when treated with a 2% THF–water mixture (Fig. S27, ESI $^{\dagger}$ ). As the control, treatment with pure water has little influence on the waveguiding property of the microwire while its optical loss begins to rise ( $>0.04\%$  v/v) and tends to reach an equilibrium state at  $\sim 0.042$   $\text{dB } \mu\text{m}^{-1}$  after  $\sim 1\%$  v/v. It is inferred that polymeric swelling of the microwire by THF changes the polymeric refractive index, and further results in the rise of the optical loss. The fluorescence intensity is quenched under interactions of THF, together with the optical loss increment of the waveguides because of evanescent-field/refractive-index change, and the above two processes actuate each other to amplify the output quenching signals and finally enhance the detection sensitivity. The detection limit of the waveguiding output is calculated to be  $\sim 0.0043\%$  v/v ( $\sim 0.53$  mM), obviously lower than that of the SU-8/gAIEoxe micropatterns ( $\sim 0.061\%$  v/v) and microwire-body ( $\sim 0.0086\%$  v/v), respectively (Table S1, ESI $^{\dagger}$ ). The excellent sensing performance of these SU-8/gAIEoxe active optical waveguides shows superior advantages in VOC sensing compared with the SU-8/gAIEoxe micropatterns and the reported solid-devices without amplified configurations. Besides, the swelling induced fluorescence dimming and optical loss increase are reversible by thermally evaporating the VOCs absorbed in these polymeric waveguides. It's measured that the microwire remains intact and reusable without any degradation, and its fluorescence intensity and optical loss change reversibly under alternate treatment of 2% THF solution immersion and 90  $^{\circ}\text{C}$  heat-treatment for 5 cycles, demonstrating the outstanding re-usability of the SU8/AIEoxe active micro/nanodevices (Fig. 5f and Fig. S25, ESI $^{\dagger}$ ).

## Conclusions

In summary, we customize three kinds of AIEgens decorated with oxetane groups used as luminous and sensing molecular transducers to lithographically fabricate polymer micro/nanodevices. The co-crosslinking of these AIEgens' oxetane groups with epoxy resins in the photoresist guarantees the high-quality lithography of highly doped AIE resins (10 wt%), and therefore improves the in-solvent stability, device formability and stimulus-responsive signals. Compared with monochromatic SU-8/AIEoxe devices, FRET fluorescent ratiometric micro/nano-sensors are constructed with three AIEoxes to optimize the accuracy and visual recognition in VOC detection. For the first time to our knowledge, SU-8/AIEoxe based microwires are customized *via* FsLDW as superior “dually smart” active optical waveguides so

that the multiple sensing mechanisms (*i.e.*, active and passive optical VOC sensing reversibly and respectively actuated by AIE fluorescence and waveguiding evanescent-field/refractive-index change) enhance each other to improve the detection limit by over one order directly in liquid phases (from  $\sim 0.061\%$  v/v (THF/water) simply *via* fluorescence to  $\sim 0.004\%$  v/v with a micro-waveguide configuration). The strategy reported here, with purposely synthesized SU8/AIEoxe composite resins and mutually enhanced multiple sensing mechanisms, constructs active optical VOC sensors with specific recognition and enhanced sensitivity, and promises novel opportunities for functional integrated optics (*e.g.*, optofluidics) for low-cost, portable, real-time and/or *in situ* organic pollutant detection and analysis.

## Conflicts of interest

There are no conflicts of interest to declare.

## Acknowledgements

The authors thank Jinlong Zhu and Song Zhu for the spectral measurements during VOC sensing. This work was supported by the National Natural Science Foundation of China (NSFC) under Grants #2017YFB1104600, #61605055, #61590930, #61825502, #81771930, and Shenzhen Science and Technology Innovation Commission (grant No. KQTD20170810111314625) and Graduate Interdisciplinary Research Fund of Jilin University (No. 10183201832).

## Notes and references

- B. B. Huang, C. Lei, C. H. Wei and G. M. Zeng, *Environ. Int.*, 2014, **71**, 118–138.
- N. S. Chary and A. R. Fernandez-Alba, *TrAC, Trends Anal. Chem.*, 2012, **32**, 60–75.
- E. Martínez, S. Lacorte, I. Llobet, P. Viana and D. Barceló, *J. Chromatogr. A*, 2002, **959**, 181–190.
- E. Louarn, A. Hamrouni, C. Colbeau-Justin, L. Bruschi, J. Lemaire, M. Heninger and H. Mestdagh, *Int. J. Mass Spectrom.*, 2013, **353**, 26–35.
- Y. Liu, K. R. Wang, D. S. Guo and B. P. Jiang, *Adv. Funct. Mater.*, 2009, **19**, 2230–2235.
- L. Zang, Y. Che and J. S. Moore, *Acc. Chem. Res.*, 2008, **41**, 1596–1608.
- R. Lu, G. P. Sheng, W. W. Li, H. Q. Yu, Y. Raichlin, A. Katzir and B. Mizaikoff, *Angew. Chem., Int. Ed.*, 2013, **52**, 2265–2268.
- C. McDonagh, C. S. Burke and B. D. MacCraith, *Chem. Rev.*, 2008, **108**, 400–422.
- R. Lu, W. W. Li, B. Mizaikoff, A. Katzir, Y. Raichlin, G. P. Sheng and H. Q. Yu, *Nat. Protoc.*, 2016, **11**, 377–386.
- D. Citterio, L. Jenny, S. Rásonyi and U. E. Spichiger, *Sens. Actuators, B*, 1997, **39**, 202–206.
- S. Dolai, S. K. Bhunia and R. Jelinek, *Sens. Actuators, B*, 2017, **241**, 607–613.
- O. Hofmann, X. Wang, A. Cornwell, S. Beecher, A. Raja, D. D. Bradley, A. J. Demello and J. C. Demello, *Lab Chip*, 2006, **6**, 981–987.
- X. Cai, N. Xie, Y. Li, J. W. Y. Lam, J. K. Liu, W. He, J. G. Wang and B. Z. Tang, *Mater. Horiz.*, 2019, **6**, 2032–2039.
- R. R. Hu, N. L. C. Leung and B. Z. Tang, *Chem. Soc. Rev.*, 2014, **43**, 4494–4562.
- J. Mei, N. L. Leung, R. T. Kwok, J. W. Lam and B. Z. Tang, *Chem. Rev.*, 2015, **115**, 11718–11940.
- G. D. Liang, F. Ren, H. Y. Gao, Q. Wu, F. M. Zhu and B. Z. Tang, *ACS Sens.*, 2016, **1**, 1272–1278.
- Y. Q. Zhang, J. H. Qiu, R. R. Hu, P. Li, L. J. Gao, L. P. Heng, B. Z. Tang and L. Jiang, *Phys. Chem. Chem. Phys.*, 2015, **17**, 9651–9658.
- G. D. Liang, F. Ren, H. Y. Gao, F. M. Zhu, Q. Wu and B. Z. Tang, *J. Mater. Chem. A*, 2017, **5**, 2115–2122.
- X. Y. Jiang, H. F. Gao, X. Q. Zhang, J. H. Pang, Y. Q. Li, K. Li, Y. C. Wu, S. Z. Li, J. Zhu, Y. Wei and L. Jiang, *Nat. Commun.*, 2018, **9**, 3799.
- X. P. Li, G. Baryshnikov, C. Deng, X. Y. Bao, B. Wu, Y. Y. Zhou, H. Agren and L. L. Zhu, *Nat. Commun.*, 2019, **10**, 731.
- H. Zhao, J. Ni, J. J. Zhang, S. Q. Liu, Y. J. Sun, H. Zhou, Y. Q. Li and C. Y. Duan, *Chem. Sci.*, 2018, **9**, 2918–2926.
- K. S. Lee, R. H. Kim, D. Y. Yang and S. H. Park, *Prog. Polym. Sci.*, 2008, **33**, 631–681.
- H. Wang, Y. L. Zhang, W. Wang, H. Ding and H. B. Sun, *Laser Photonics Rev.*, 2017, **11**, 1600116.
- Y. L. Sun, Q. Li, S. M. Sun, J. C. Huang, B. Y. Zheng, Q. D. Chen, Z. Z. Shao and H. B. Sun, *Nat. Commun.*, 2015, **6**, 8612.
- D. X. Liu, Y. L. Sun, W. F. Dong, R. Z. Yang, Q. D. Chen and H. B. Sun, *Laser Photonics Rev.*, 2014, **8**, 882–888.
- R. Taniguchi, T. Yamada, K. Sada and K. Kokado, *Macromolecules*, 2014, **47**, 6382–6388.
- L. Liu, M. Wang, L. X. Guo, Y. Sun, X. Q. Zhang, B. P. Lin and H. Yang, *Macromolecules*, 2018, **51**, 4516–4524.
- X. F. Fang, X. Z. Chen, R. Q. Li, Z. H. Liu, H. B. Chen, Z. Z. Sun, B. Ju, Y. F. Liu, S. X. Zhang, D. Ding, Y. J. Sun and C. F. Wu, *Small*, 2017, **13**, 1702128.
- A. d. Campo and C. Greiner, *J. Micromech. Microeng.*, 2007, **17**, R81–R95.
- M. Sangermano, R. Bongiovanni, G. Malucelli, A. Priola, R. R. Thomas, R. E. Medsker, Y. Kim and C. M. Kausch, *Polymer*, 2004, **45**, 2133–2139.
- H. B. Chen, K. W. Chang, X. J. Men, K. Sun, X. F. Fang, C. Ma, Y. X. Zhao, S. Y. Yin, W. P. Qin and C. F. Wu, *ACS Appl. Mater. Interfaces*, 2015, **7**, 14477–14484.
- A. Dubois, M. Canva, A. Brun, F. Chaput and J. P. Boilot, *Appl. Opt.*, 1996, **35**, 3193–3199.
- W. Yao, M. Tebyetekerwa, X. H. Bian, W. Li, S. Y. Yang, M. F. Zhu, R. Hu, Z. M. Wang, A. J. Qin and B. Z. Tang, *J. Mater. Chem. C*, 2018, **6**, 12849–12857.
- H. Zhou, F. Liu, X. B. Wang, H. Yan, J. Song, Q. Ye, B. Z. Tang and J. W. Xu, *J. Mater. Chem. C*, 2015, **3**, 5490–5498.
- Y. S. Zhou, L. Zhang, H. Y. Gao, F. M. Zhu, M. L. Ge and G. D. Liang, *Sens. Actuators, B*, 2019, **283**, 415–425.
- H. S. Peng, J. A. Stolwijk, L. N. Sun, J. Wegener and O. S. Wolfbeis, *Angew. Chem., Int. Ed.*, 2010, **49**, 4246–4249.

- 37 L. Chen, J. W. Ye, H. P. Wang, M. Pan, S. Y. Yin, Z. W. Wei, L. Y. Zhang, K. Wu, Y. N. Fan and C. Y. Su, *Nat. Commun.*, 2017, **8**, 15985.
- 38 Y. L. Sun, S. M. Sun, P. Wang, W. F. Dong, L. Zhang, B. B. Xu, Q. D. Chen, L. M. Tong and H. B. Sun, *Small*, 2015, **11**, 2869–2876.
- 39 L. Li, H. T. Lin, S. T. Qiao, Y. Z. Huang, J. Y. Li, J. Michon, T. Gu, C. Alosno-Ramos, L. Vivien, A. Yadav, K. Richardson, N. S. Lu and J. J. Hu, *Light: Sci. Appl.*, 2018, **7**, 17138.
- 40 J. H. Chen, J. Tan, G. X. Wu, X. J. Zhang, F. Xu and Y. Q. Lu, *Light: Sci. Appl.*, 2019, **8**, 1–8.
- 41 E. J. Wang, J. W. Y. Lam, R. R. Hu, C. Zhang, Y. S. Zhao and B. Z. Tang, *J. Mater. Chem. C*, 2014, **2**, 1801.
- 42 G. Yang, W. L. Hu, H. Y. Xia, G. Zou and Q. J. Zhang, *J. Mater. Chem. A*, 2014, **2**, 15560.
- 43 Y. K. Che, X. M. Yang, S. Loser and L. Zang, *Nano Lett.*, 2008, **8**, 2219–2223.